Full Length Article

Factors controlling conductivity of PEDOT deposited using oxidative chemical vapor deposition

Grant Drewelow[b], Han Wook Song[c], Zhong-Tao Jiang[d], Sunghwan Lee[a],[*]

[a] School of Engineering Technology, Purdue University, West Lafayette, IN 47907, USA
[b] Department of Mechanical Engineering, Baylor University, Waco, TX 76798, USA
[c] Center for Mass and Related Quantities, Korea Research Institute of Standard and Science, Daejeon 34113, South Korea
[d] School of Engineering and Information Technology, Murdoch University, Murdoch, WA 6150, Australia

ABSTRACT

This study is aimed to enhance the understanding of the processing-structure-property relationship in oxidative chemical vapor deposition (oCVD) conjugated polymers. Particular focus is made on the substrate and oxidant temperatures for the oCVD poly(3 4-ethylenedioxythiophene) (PEDOT) growth and their effects on the structure and electrical properties on resulting thin films. Doping levels are evaluated using Fourier-transform infrared spectroscopy and x-ray photoelectron spectroscopy, which is complemented by Hall Effect investigations. Further, the relationship between doping level and conjugation length is described with discussion on mean free path, where the mean free path of oCVD PEDOT (up to ~5 nm) is significantly larger than typical organic semiconductors and comparable to conventional inorganic counterparts. The mechanisms that govern oCVD film growth are suggested, which is strongly dependent on both substrate and oxidant sublimation temperatures. Finally, the carrier transport behaviors, dominated by conjugation and doping levels are discussed.

1. Introduction

Conjugated polymers that show electrical conductivity and mechanical flexibility have been attracting lots of attention due to their potential applications in flexible electronic and optoelectronic devices. Conductive polymers consist of a network of alternating single and double carbon bonds, which result in conjugated π-bonds that lead to electrical conductivity in materials. Various types of conjugated polymers including polyaniline, polypyrrole, poly(3,4ethylenedioxythiophene) (usually abbreviated as PEDOT) and their derivatives have been actively investigated [1–5]. Among conjugated polymers, PEDOT has been gaining particular attention from the academic and industrial communities due to its stability, visible-regime light transmission, processability and high conductivity, relative to other conjugated polymers.

As a conventional technique, solution processing has been widely utilized to grow conjugated polymer films like many other polymers [6,7]. PEDOT has been prepared through solution-phase processing as well, in the form of PEDOT:PSS [7–9] where polystyrene sulfonate (PSS) works as a dopant and also as a medium to endow solubility to PEDOT, enabling solution processing. PEDOT:PSS films coated from commercially procured formulation demonstrate a conductivity of ~650 S/cm or higher. However, in the solution-based growth of PEDOT:PSS, the surface hydrophobicity is essential, which makes processing unavailable and complicated in many cases. Efforts have been made to resolve wetting issues of PEDOT:PSS by employing O_2 plasma treatment on substrates before applying solution processes [10] or by using the captive bubble technique [11]. These additional steps using a high energy source of plasma or liquid bubbles destroy or damage the underlying substrate properties.

Vapor phase polymerization (VPP) techniques have also been previously used for preparing conjugated polymer films. For example, plasma enhanced CVD was used to polymerize monomers of thiophene, pyrrole and aniline and their derivatives; however, the resulting polymers often lack conductivity and the regular repeat units found in conventional polymers due to the harsh deposition conditions (e.g., energetic and nonselective plasma polymerization process) [12–15]. VPP process was also used for oxidative polymerization of conjugated polymers, which critically relies on solvent casting of the oxidants (e.g., PSS or iron (III) tosylate) prior to exposure of monomer vapor [16–18]. Solution casting required for VPP can deteriorate underlying layers/substrates and make conformal, non-destructive deposition on many substrates challenging, similarly as discussed for solution-processed polymer growth.

Oxidative chemical vapor deposition (oCVD) differs from VPP, particularly in the oxidant delivery method. Unlike VPP, which requires a solution containing an oxidizing agent, or solution-based polymerization necessitating monomer solubility, the oCVD technique does not require solution-casted oxidants, solubility in solvents or solution compatibility with substrates and underlying layers. The solvent-free oCVD polymerization enables the deposition of conjugated polymer films on virtually any substrate and leads to greater film uniformity over large areas [19,20], enhanced electrical properties (e.g., conductivity [20], mobility [21]) and excellent conformality for non-planar [22,23] and patterned [24,25] structures. The oCVD films have been demonstrated as channel layers in field effect transistors [26,27], transparent conductors for electrodes [22], hole transport layers [28,29] in organic solar cells, stimuli-responsive layers in sensors [30–32]. Moreover, oCVD offers various processing benefits including excellent large-area homogeniety and its potential for inline integration with other standard manufacturing vacuum processes [33].

Processing conditions are significant factors to control chemical, crystallographic and micro structures of thin film materials and the resulting structures dominate overall properties of materials. Therefore, an understanding of materials' processing-structure-property relationship is critical to achieve the characteristics relevant to specific applications. Of the processing conditions, in the presenst study, the focus was made on the effects of substrate and oxidant temperatures on the structures (chemical, crytallographic and micro patterns) and the electrical properties of PEDOT films. Particularly, it has been shown that the substrate temperature is one of the dominating factors to conclude the performance of the resulting oCVD polymeric films [34,35]; however, the effect of oxidant sublimation temperature has yet to be reported for oCVD polymerizations. The structures were evaluated using atomic force microscopy, x-ray diffraction, Fourier-transform infrared spectroscopy and x-ray photoelectron spectroscopy. The electrical properties were investigated using a four-point probe and a Hall Effect system. Through the series of measurements, the growth rate behavior and the factors controlling doping level and conductivity were studied. The carrier transport behaviors were also discussed in regards to conjugation length and mean free path of the carriers.

2. Experimental details

For the synthesis and depositions of PEDOT films, commercially procured EDOT ($\geq$97%, Sigma-Aldrich) and iron (III) chloride (FeCl$_3$, 97%, Sigma-Aldrich) were used as purchased. Glass slides and silicon wafers were used as substrates. PEDOT films were deposited using oxidative chemical vapor deposition (oCVD) in a custom-built reactor. In order to achieve a base pressure below 5×10^{-5} Torr, a dual vane mechanical pump (Leybold D65BCS) and a turbo-molecular pump

(Pfeiffer Vacuum) were employed. During oCVD depositions, a working pressure of approximately $4–8 \times 10^{-3}$ Torr was maintained by controlling a monomer feed rate through a butterfly-type throttling valve.

The oxidizing agent, FeCl$_3$, and its crucible was heated from room temperature to target temperatures ranging 140–250 °C at a slow ramping rate of ~2–3 °C/min in order to prevent the oxidants from abrupt spring-forth inside the chamber. The substrate stage was rotated at a rate of 5 rpm during the depositions to ensure the film uniformity. The reactor body was heated to 150 °C in order to provide a favorable chemical reaction environment and also to prevent the synthesized polymers from being deposited on the chamber wall. After deposition, the samples were all sequentially rinsed in methanol for > 5 mins and 0.2 M HCl for > 5 mins to wash out reacted and residual oxidant, followed by air-dry in a fume hood for longer than 10 mins.

Surface morphologies and root mean square roughness of the synthesized thin films were measured using atomic force microscopy (AFM, Veeco Multimode with Nanoscope V) in tapping mode with a Bruker Si cantilever (tip frequency of 330 kHz). The x-ray diffraction (XRD) measurements were taken using the glancing incident angle technique in a Siemens D5000 diffractometer, with Cu Kα radiation (λ = 1.54 Å) at 40 kV and 40 mA. The electrical conductivity of oCVD PEDOT films were evaluated using a four point probe (custom-built probe station with a Keithley 2000 digital multimeter) and a Hall Effect measurement system (GMW Associates). The carrier concentration and the carrier mobility were also characterized from Hall Effect measurements with a small current source of ~1 nA and the source current and the specimen voltage were recorded using a Keithley 4200A-SCS parameter analyzer with input impedance greater than 1 TΩ. A magnetic field of 5200 Gauss from a C-frame electromagnet (GMW Associates) with a bipolar power supply (KEPCO Inc.) was used throughout the Hall measurements. Film thicknesses were measured using an FS1multi-wavelength ellipsometer (Film Sense) at an incident and detection angle of 65°. X-ray photoelectron spectroscopy (XPS) analysis was made to investigate elemental compositions and doping levels in the PEDOT films using a Thermo Scientific K-Alpha XPS spectrometer under high vacuum ($< 10^{-8}$ Torr) with focused monochromatic Al Kα X-ray radiation at 1486.7 eV. An electron flood gun was also used for the XPS measurements in order to prevent charge accumulation on the surface of the thin films. An angle of 55° from the surface normal was used in this study to collect photoelectrons. Fourier transform-infrared spectroscopy (FTIR) spectra were obtained from oCVD PEDOT films deposited on Si wafers to investigate an IR spectrum of absorption and chemical bonding properties using an iS5 FTIR with ATR mode (Thermo Fisher Scientific).
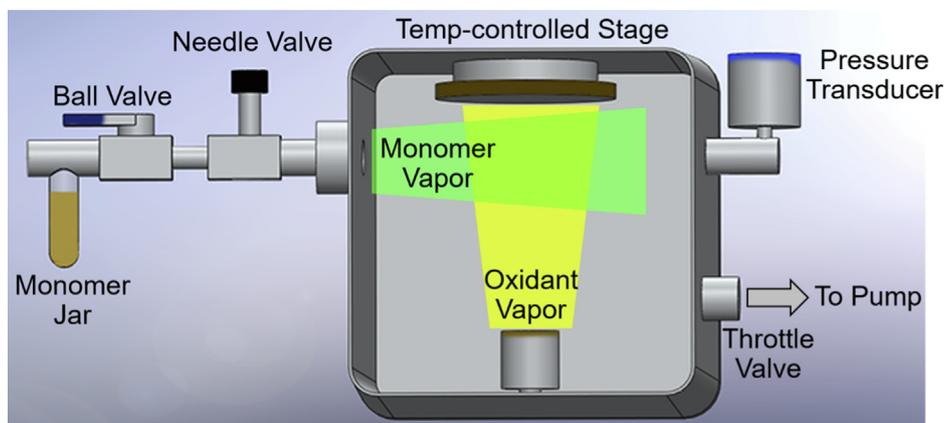
Fig. 1. Schematic of oCVD reactor: EDOT monomer is vaporized in a monomer jar outside the chamber and introduced to the reactor. Solid phase oxidants (FeCl$_3$ in this study) is sublimated inside the chamber. Synthesized PEDOT is deposited on a temperature controlled and rotating substrate.

3. Results and discussion

Oxidative chemical vapor deposition (oCVD) has uniquely demonstrated a simple and easy synthesis and deposition of conjugated polymers at low temperatures (20–150 °C) [20,25]. Fig. 1 schematically describes the oCVD apparatus and its unique abilities for the synthesis, deposition and doping of PEDOT conjugated polymers in a single step process. The precursor, EDOT monomer is vaporized at 140 °C from a temperature-controlled glass jar outside of the reactor and introduced in the gas phase into the chamber through an inlet port. The oxidizing agent, $FeCl_3$, which works as dopant and step growth initiator, is sublimated from a crucible, heated by a point source evaporator in the chamber at temperatures ranging from 140 to 250 °C. EDOT monomer vapors reacted via oxidative polymerization with the sublimated oxidizing agent to yield solid polymer films on the stage. The oCVD synthesis of PEDOT follows the well-known step-growth mechanism which describes the evolutions of steps of oxidation of EDOT to from cation radical; dimerization; deprotonation to form conjugation; further polymerization from n-mer to (n + 1)-mer; doping PEDOT [34,35]. The substrate stage is at the top of the reactor chamber and inverted to face down. During the oCVD process, the upward direction deposition provides greater uniformity and higher electrical conductivity of conjugated polymers compared to that of bottom-substrate configuration [35]. The stage is capable of rotating, which further contributes to improved uniformity of resulting films over the 4 in. size of substrates.

Fig. 2 compares the effect of oxidant temperature (T_{oxi}) on the growth rate and the growth rates are plotted on an Arrhenius plot. In Fig. 2(a) for a substrate temperature of room temperature (RT, no intentional heating), the growth rate monotonically increases with increasing oxidant temperature from approximately 0.7 nm/min (T_{oxi} = 140 °C) to a high growth rate of ~40 nm/min (T_{oxi} = 250 °C) and no saturation behavior in growth rate is observed. This monotonic increase in growth rate can be understood by the reaction-rate limited mechanism, explaining that at low reaction temperatures or high vacuum, the reaction rate is below the gas arrival rate. In the reaction-rate limited growth, temperature (T_{oxi} in this investigation) controls film deposition rate as shown in Fig. 2(a). However, in Fig. 2(b), a change in growth mechanism is evidently observed: the growth rate at a substrate temperature, T_{sub} = 50 °C shows a clear saturation behavior (approximately 4 nm/min) at T_{oxi} higher than 180 °C while at lower temperatures, the growth rate increases with T_{oxi} as similarly shown in Fig. 2(a). For the growth rate of T_{sub} = 50 °C, at lower T_{oxi}, the polymerization reaction-rate governs the growth rate; however, with increasing T_{oxi} another mechanism, known as mass-transport limited process dominates the oCVD PEDOT growth due to higher vapor pressure at higher

T_{sub}, which limits surface adsorption to be deposited on the substrate surface. The growth rate at T_{sub} = 100 °C is shown in Fig. 2(c) where the growth rate of oCVD PEDOT remains nearly constant at a rate of approximately 1 nm/min at all temperatures investigated in this study, which indicates that at higher T_{sub}, the effect of T_{oxi} is insignificant because the surface adsorption is critically limited because of quite high vapor pressure (i.e., mass-transport limited mechanism). Overall, in these growth rate investigations, it should be noted that (1) substrate temperatures dominate the overall growth rate: lower substrate temperatures lead to a higher growth rate than those deposited at higher substrate temperatures, which is simply understood by a lower vapor pressure of the vaporized monomer at lower temperatures; and (2) oxidant vaporizing temperature is the second governing factor controlling the growth rate because higher T_{oxi} provides greater amount of oxidant vapor that initiates the step growth polymerization [36]. The activation energy for the growth rate change, extracted from the Arrhenius plots, is found to be 1.92 eV for PEDOT grown at T_{sub} = RT and 3.44 eV for PEDOT, T_{sub} = 50 °C for the linear regime, of which the values are in the range of general CVD growth rate, 1–4 eV [37,38]. As expected from the growth rates shown in Fig. 2(a) and (b), the higher activation energy indicates that larger energy is required to increase the growth rate for PEDOT at higher substrate temperatures.

In order to investigate amorphous/crystalline structure of the resulting oCVD PEDOT films, x-ray diffraction (XRD) measurements were made on the PEDOT films grown on glass slide substrates with a thickness of 50 nm. Glancing incident angle XRD was performed in the 2 theta scan mode at a fixed incident angle of approximately 1° to enhance x-ray penetrating distance for the thin films, which, in turn, provides meaningful diffraction intensity compared to noise levels. Fig. 3 shows the typical XRD spectra of the PEDOT samples deposited at substrate temperatures of RT (bottom), 50 °C (middle) and 100 °C (top). An evident crystalline peak is clearly seen at a diffraction angle, 2 theta of approximately 6.51° for all the PEDOT films, even for the one deposited at room temperature, while the diffraction intensity increases with increasing substrate temperature during the oCVD deposition. The peak is a characteristic crystalline peak of (h00) planes for PEDOT observed for both solution processed PEDOT:PSS [39] and oCVD PEDOT [36] in which PEDOT polymer chains have crystallographic orders in an edge-on stacking orientation [36]. Recently, Wang *et al.* [36] reported that the oCVD is able to tune the crystalline orientation of PEDOT with a systematic control of film thickness and processing substrate temperature. It was found that in oCVD processing, very thin PEDOT layer (< ~15 nm) and high substrate temperature (T_{sub} > ~250 °C) conditions lead to a dominant phase with face-on orientation, and thicker films and lower temperature depositions yield
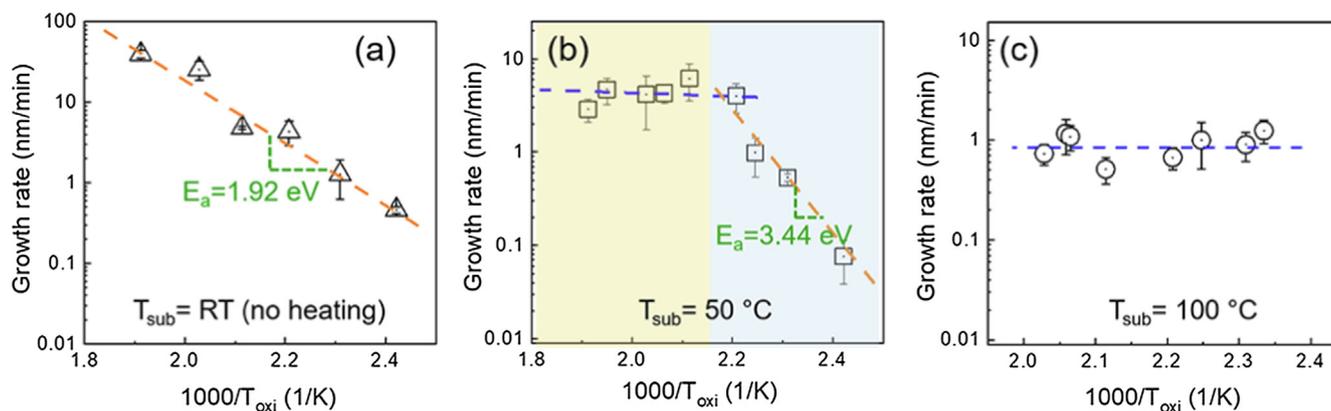
Fig. 2. Effect of oxidant temperature (T_{oxi}) on the PEDOT growth rate as a function of substrate temperature (T_{sub}) during oCVD depositions: (a) at T_{sub} = RT (low temperatures in general), the growth rate increases monotonically with increasing T_{oxi} with an activation energy (E_a) of 1.92 eV, (b) at T_{sub} = 50 °C, the growth rate increases at low T_{sub} with E_a of 3.44 eV; however, at higher T_{oxi}, the growth rate is nearly constant, and (c) at T_{sub} = 100 °C, the growth rate is nearly constant at all investigated T_{oxi} (i.e., independent of T_{oxi}). This oCVD PEDOT growth-rate study reveals that (1) T_{sub} is the primary factor for the growth rate since Tsub governs the vapor pressure for the polymerization at the substrate and (2) T_{oxi} is the second dominating factor, controlling the growth rate.
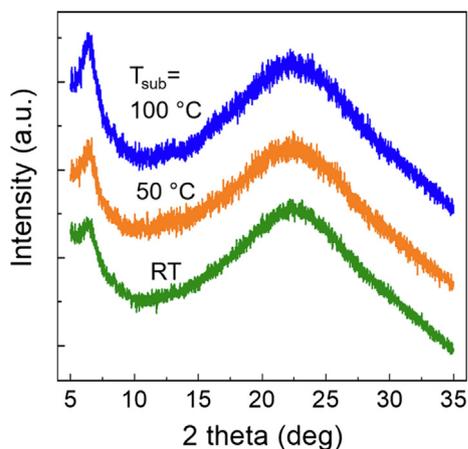
Fig. 3. X-ray diffraction spectra of oCVD PEDOT films showing the characteristic PEDOT peak at a diffraction angle of 6.51° due to crystalline (h00) planes. The crystalline structure is enhanced with increasing T_{sub}, which indicates that more ordered crystalline phase prevails in oCVD PEDOT prepared at higher T_{sub}. This enhanced ordered structure is related to the longer polymer conjugation, contributing to carrier transport (will be discussed in more detail later with FTIR, electrical property measurements and XPS.).

an edge-on stacking orders. In this work, for practical transparent electrode and flexible device applications, temperatures up to 100 °C and thickness 50–100 nm were considered for XRD analysis and the resulting crystalline orientation of PEDOT shown in Fig. 3 is found to be in edge-on stacking, which is in good agreement with the finding by Wang *et al.* [36]. The glass substrate also appears as the broad amorphous peak in the spectra in the range of 15° < 2θ < 35°.

AFM surface morphological images are shown in Fig. 4 as a function of substrate temperature. Clear changes in the three-dimensional images were observed: with increasing substrate temperature, the size of grain-like features in the PEDOT films increases and, in turn, the root-mean-square roughness (R_{rms}) increases from 1.71 nm (RT) to 3.18 nm (T_{sub} = 50 °C) and 6.93 nm (T_{sub} = 100 °C). The increase in roughness at higher substrate temperatures is likely attributed to enhanced crystalline structures and larger grain size as shown in the XRD spectra in Fig. 3. Longer chain conjugation at higher T_{sub}, which leads tighter and more networked chain structure, would also results in the increase in roughness for PEDOT samples grown at higher T_{sub}. Further details on conjugation length of PEDOT as a function of substrate temperature will be discussed later in this report.

Fig. 5 shows the spectra of the Fourier transform infrared (FTIR) spectroscopy. The obtained FTIR spectra of PEDOT shows similar primary features as previously reported oCVD PEDOT [34,35] and solution processed PEDOT(:PSS) films [40,41]. Although detailed quantitative analysis is limited due to the broadness and peak overlaps/shifts, the FTIR results still deliver important aspects of oCVD PEDOT regarding
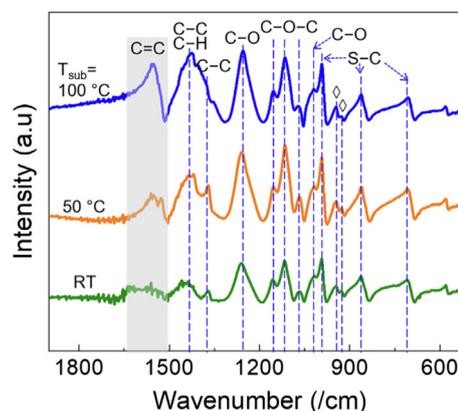
Fig. 5. FTIR absorption spectra with peak indexes for oCVD PEDOT as a function of T_{sub}: enhanced peak intensity and peak broadness are clearly seen, particularly at ~1600–1500/cm from C=C stretching in the thiophene ring and ~1500–1350/cm from C—C stretching and C—H bending, indicating an increase in conjugation and doping level with increasing T_{sub}.

conjugation and doping as a function of growth substrate temperature. The peak at approximately 1533 cm^{-1} is associated with stretching modes of C=C bond in the thiophene ring [40,41] while the peak at ~1430 cm^{-1} is attributed to the C—C stretching and C—H bending. A shoulder appears at 1370 cm^{-1} on the right side of the peak at 1430 cm^{-1}, which is attributed to the C—C stretching mode as well. Note that the resulting FTIR absorption spectra clearly show that the peak intensity at ~1533 cm^{-1} correlating C=C stretch increases with increasing T_{sub}. Since an increase in absorption intensity of C=C stretch at ~1533 cm^{-1} indicates longer conjugation length [35] and higher doping in PEDOT [35], the FTIR results suggest that the doping level of PEDOT films grown at higher substrate temperature is greater than that of lower T_{sub} PEDOT. The peak broadness shown at the wavelength between 1511 and 1313 cm^{-1} is also attributed to the increased doping level since the infrared absorption increases with increasing carriers within the band gap and/or near the band edge and therefore, broader peaks refer to higher doping level and longer conjugation length in conducting polymers. Initially two distinctive peaks at 1430 and 1370 cm^{-1} (the shoulder peak) in PEDOT with T_{sub} = RT become larger and are merged at higher temperatures due to the effect of increased doping and conjugation. Other peaks are also clearly visible: the vibrations of C—S bond [40,41] in the PEDOT chains are observed at ~989, 861 and 701 cm^{-1}. The bands at ~1164, 1122, and 1064 cm^{-1} correspond to C—O—C bond stretching from the ethylenedioxy group [40,41], and the band near 944 and 927 cm^{-1} is due to the deformation mode of the ethylenedioxy ring [41]. The C—O bond stretch [40] is seen at ~1254 and 1027 cm^{-1}. Although the FTIR measurements were made on samples with a similar thickness, the peak intensities of PEDOT, T_{sub} = RT are lower than those in the higher T_{sub} PEDOT films due to
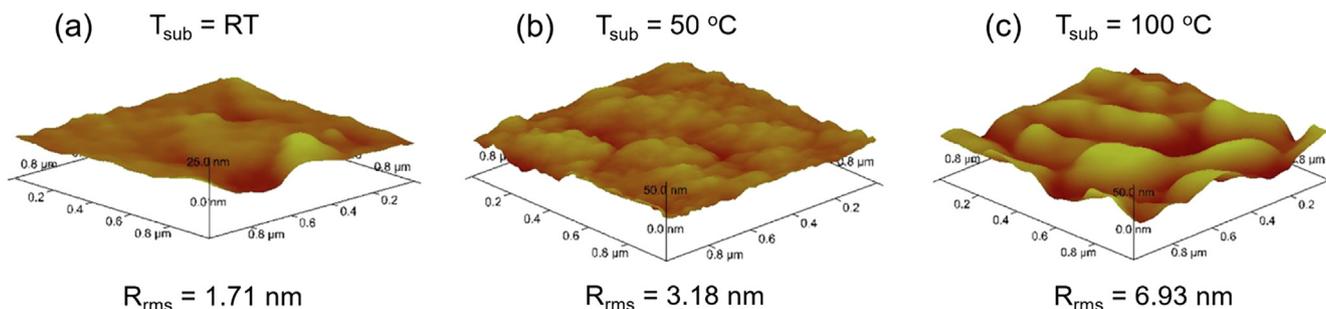
Fig. 4. AFM topographic images of oCVD PEDOT films measured in the area of 1 μm × 1 μm using tapping mode whose roughness is approximately 1.71 nm, 3.18 nm and 6.93 nm of PEDOTs grown at T_{sub} = (a) RT, (b) 50 °C and (c) 100 °C, respectively. The increased roughness is likely attributed to larger grain size, resulting from the enhanced crystalline structure shown in the XRD spectra.
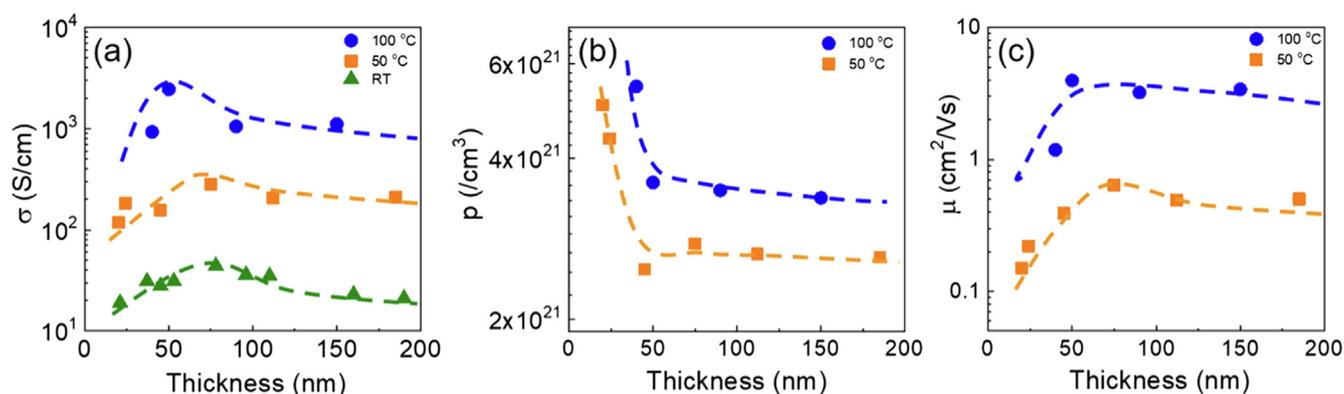
Fig. 6. Electrical properties measured using a Hall Effect system as a function of T_{sub} and film thickness: (a) conductivity, (b) carrier density and (c) carrier mobility. The conductivity increased with increasing T_{sub}; however, as a function of thickness, conductivity plots show an initial increase and a slight decrease/saturation. This overall conductivity is attributed to (1) a change in carrier density with thickness presenting an initial decrease and a saturation, and (2) a mobility trend showing initial increase and a slight decrease/saturation while the change in mobility is greater than that of carrier density.

ineffective doping and conjugation during the oCVD growth.

Electrical properties of conductivity, carrier density and carrier mobility were measured using a four-point probe and a Hall Effect measurement system in the van der Pauw configuration. Fig. 6(a) shows the overall conductivity trend of oCVD PEDOT films as a function of substrate temperature and thickness. Higher substrate temperature leads to a higher conductivity of PEDOT films (max 44, 280 and 2,447 S/cm achieved for the substrate temperatures of RT, 50 °C and 100 °C, respectively). Note that the conductivity of all the samples initially increases and after reaching the maximum value, the conductivity decreases with increasing film thickness. The initial increase can be understood by the surface scattering of the charge carriers (holes in PEDOT) which limits the carrier transport that is commonly observed in many electronic thin film materials including metals, oxides and polymers [42]. In general, the surface scattering effect on the conductivity gets weaker when thin films become thicker and the electrical properties of films approach to the bulk properties, which is opposite to the trend shown in this PEDOT study. The later decrease in conductivity is attributed to an increase in the density of defects and impurities. Our previous study reported that thicker samples contain more impurities than thinner films such as residual oxidants after rinsing, which works as additional scatter centers [43,44]. Further, it has also been reported that the degree of polymer chain disorder increases with increasing film thickness, which limits the carrier transport in PEDOT [44,45].

Hall Effect measurements allow for the separate investigation of carrier density and carrier mobility. The results from PEDOT films deposited at 50 °C and 100 °C are shown in Fig. 6(b) and (c), where the results for $T_{sub} = RT$ are excluded since inconsistent values were obtained possibly due to very low carrier mobility in the $T_{sub} = RT$ samples. While the carrier density in Fig. 6(b) is found to be very high, on the order of $10^{21}/cm^3$ in all the PEDOT films, higher carrier density was achieved at higher substrate temperatures which is in a good agreement with the FTIR results in Fig. 5 that shows longer conjugation length in PEDOT films grown at higher temperatures. Note that the carrier density decreases with increasing film thickness, which matches with the discussion above regarding the higher concentration of residual oxidizing agents that reduce the free carrier density [43]. Detailed analysis and discussion on the mechanism for the reduction in carrier density can be found in our previous study [43]. The carrier mobility of PEDOT films is shown in Fig. 6(c) where the carrier mobility of PEDOT grown at a higher substrate temperature is greater than that for the PEDOT with lower T_{sub}. The mobility increases with increasing film thickness of which the behavior reflects well the surface scattering effect for the charge carriers, which was described with the conductivity in Fig. 6(a).

In Fig. 7, a set of carrier mobility vs. carrier density (p) for the oCVD PEDOT films, which are adapted from Fig. 6, are plotted in log-log
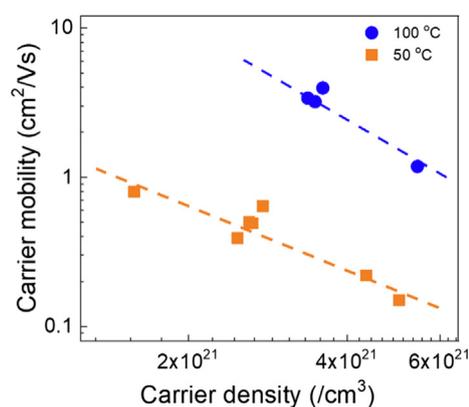
Fig. 7. Plot of carrier density vs carrier mobility of oCVD PEDOT films which provides the carrier transport behaviors: (1) an increase in carrier density leads to a decrease in carrier mobility associated with an increase in ionized impurity scattering events and (2) longer conjugation and greater ordered structure achieved through higher T_{sub} deposition results in enhanced carrier mobility due to the favored and longer carrier transport paths provided.

scales. The plot explicates the two significant carrier transport behaviors between mobility and carrier density. (1) First, in both curves, it is clearly shown that the higher carrier density results in lower carrier mobility. In PEDOT films grown at 50 °C, for example, carrier mobility decreases from approximately $1\,cm^2/V{\cdot}s$ at $p = 1.5 \times 10^{21}/cm^3$ to $\sim0.2\,cm^2/V{\cdot}s$ at $p = 5.1 \times 10^{21}/cm^3$. A similar trend is seen for PEDOT grown at 100 °C where relatively high carrier mobility of $\sim5\,cm^2/V{\cdot}s$ at $p = 3.6 \times 10^{21}/cm^3$ is observed for PEDOT grown at 100 °C, and then the mobility decrease to $1.2\,cm^2/V{\cdot}s$ at higher carrier density of $5.4 \times 10^{21}/cm^3$. The change in carrier mobility can be understood to be an ionized impurity scattering occurring between charge carriers and counter-ions, which is the mechanism by which heavy-doping limits the carrier mobility. In the present study, and for other thiophene-based oxidative polymerizations (not only for oCVD polymers [26,36,43] but also conventional solution-processed polymers [6]), iron chloride ($FeCl_3$) is one of the most wieldy used oxidizing agents. During the step-growth polymerization for PEDOT, the oxidizing agent scavenges one electron per molecule and becomes a negatively charged ion (i.e., dopant counter anion, $FeCl_4^-$ or Cl^-) by which one positively charged free carrier (i.e., hole) is generated in the polymer chains. This means that the counter anion density also increases with increasing doping concentration to achieve highly conducting PEDOT. The anions work as additional scattering centers due to the electrostatic Coulomb interactions between, in this study, positive charges (holes) and negative charges (ionized impurities, $FeCl^{4-}$ or Cl^-). This ionized impurity
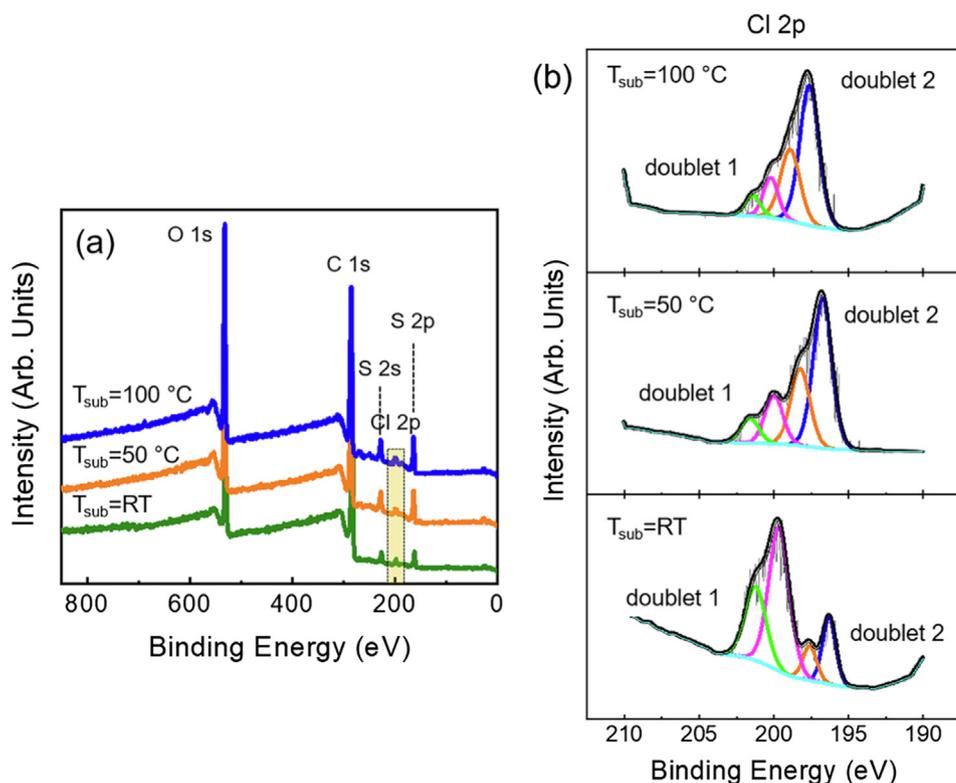
Fig. 8. XPS investigations of oCVD PEDOT films: (a) survey scans in the BE range of 0 to 850 as a function of T_{sub} showing similar spectra to each other for the peaks from O, C, S and Cl and (b) core-level high resolution (HR) XPS spectra of Cl 2p. Although all the HR spectra of Cl 2p show two doublets, the ratio between the two doublets significantly changes: with increasing T_{sub}, the intensity and area of doublet 1 (from C−Cl species) decreases; however, the intensity and area of doublet 2 from (dopant counter ions) increases, which describes the doping level increases with increasing T_{sub}.

scattering mechanism explains a decrease in carrier mobility with increasing carrier density, particularly for heavily-doped materials, like the PEDOT in this study with high carrier density $> 10^{21}/cm^3$ [43].

(2) Second, greater mobility is obtained for PEDOT with longer conjugation length. Since conjugated polymer chain works as charge carrier transport paths, longer conjugation results in higher carrier mobility. Although a direct determination of conjugation length of PEDOT is not available due to the insoluble nature of PEDOT, comparison of the mean free path between the PEDOT films provides significant insights on the degree of carrier transport which is directly related to conjugation length. The mean free path (L) of the charge carrier is determined by the equation [46]:

$$L = \frac{3\pi\sigma h}{2q^2 k_F^2} = \frac{h}{2q}(3\pi p)^{(1/3)}\mu \tag{1}$$

where, h is the Planck constant, k_F the Fermi wave-vector which is defined as $k_F = (3\pi p)^{1/3}$, q the unit charge of electron and μ the carrier mobility. The calculated mean free path values of the oCVD PEDOT films are approximately 0.31–0.82 nm for PEDOT, $T_{sub} = 50\,°C$ and 4.25–5.30 nm, increased about an order of magnitude, for PEDOT, $T_{sub} = 100\,°C$. The values of the mean free path is found to be considerably higher than those of many organic semiconductors that are comparable or even lower than the intermolecular spacing (i.e., < few angstroms) at room temperature [47,48]: for example, an organic molecule of single crystalline oligoacene (< 0.1 nm, general disordered oligoacene results in much lower mean free path) [47] and other conjugated polymer of unsubstituted polythiophene ($\sim 10^{-5}$ nm) [46]. It is generally believed that the very short mean free path for organic semiconductors is due to charge carriers that need to hop from energy states to adjacent available energy states for conduction, reported on many other organic and polymeric semiconductors [46,49–53]. Note, however, that the mean free path values extracted for the oCVD PEDOT films are on the order of a few nanometers, which are comparable or slightly less than those (~ 1–50 nm) of conventional inorganic semiconductors in single- or poly-crystalline states such as Si [54] and transition metal oxides (e.g., ZnO) [55]. This mean free path

investigation complements the qualitative analysis regarding the degree of conjugation of PEDOT and is in a great agreement with the FTIR results shown in Fig. 5.

XPS survey scans and core-level high resolution (HR) spectra provide the chemical environment of oCVD PEDOT films and the doping state as a function of substrate temperature. All the survey scans of the PEDOT films of $T_{sub} = RT$ (bottom), 50 °C (middle) and 100 °C (top) are shown in Fig. 8(a) with binding energies ranging from 0 to 850 eV where the three spectra are similar to each other. Considerable peaks from O, C, S and Cl were seen in the survey scans while the intensity of the S-related peaks in PEDOT grown at RT is less than those in PEDOT grown at higher temperatures, which is reasonably attributed to the less conjugation compared to the higher T_{sub} PEDOT films. The XPS investigation regarding conjugation length is well matched with the FTIR results in Fig. 5 and the discussion about the mean free path pertaining to Fig. 7. Core-level high resolution XPS spectra of Cl 2p are given in Fig. 8(b) for the PEDOT films of $T_{sub} = RT$ (bottom), 50 °C (middle) and 100 °C (top). For the HR Cl 2p spectra in Fig. 8(b), two spin-orbit splitting doublets of Cl $2p_{3/2}$ and Cl $2p_{1/2}$ (i.e., doublet 1 and 2) are seen with the binding energy difference of approximately 1.6 eV and the two Cl $2p_{3/2}$ peaks are found at binding energies of approximately 200.8 (doublet 1) and 198.4 eV (doublet 2), which is well matched with other thiophene-based polymers oxidized (i.e., doped) with $FeCl_3$ and other Fe/Cl-based dopants [6,46,56]. The intensity ratio, 2:1 between each doublet of Cl $2p_{3/2}$ and Cl $2p_{1/2}$ is maintained as typical Cl species [46,57] due to spin-orbit coupling effects in the final state of the emitted electron [58–60]. The doublet 1 components with Cl $2p_{3/2}$ at BE 200.8 eV and Cl $2p_{1/2}$ at 202.4 eV result from the C−Cl species, due to the chlorination of the polymer backbone during oxidative polymerization [61]. The components of doublet 2, consisting of Cl $2p_{3/2}$ at 198.4 eV and Cl $2p_{1/2}$ at 199.9 eV, are associated with the dopant counter ions of Cl^- and $FeCl_4^-$ [61,62]. It should be noted, however, that considerable changes in peak intensity are observed between doublets 1 and 2 as substrate temperatures increase: the bottom spectrum for the PEDOT film, $T_{sub} = RT$ shows the strong components for doublet 1 whose aerial portion of the total Cl 2p scan is 76.5% of total

Cl species and the rest, 23.5% is ascribed to doublet 2. The HR XPS curves for the PEDOT films grown at higher T_{sub} clearly present a significant increase in peak intensity for doublet 2 (76.6% and 83.9% for PEDOT films, T_{sub} = 50 °C and 100 °C, respectively), pertaining to the amount of counter anions (Cl- and $FeCl_4{}^-$). Therefore, the increase in peak intensity of doublet 2 for the higher T_{sub} PEDOT films indicates much greater doping (> three-fold increase) than that in PEDOT, T_{sub} = RT. This XPS analysis of oCVD PEDOT, which describes the effect of substrate temperature on doping, is in good agreement with the previous discussion with the FTIR results and electrical properties.

4. Conclusion

The focus of the present study is to provide an enhanced understanding of the processing-structure-property relationship in oxidative chemical vapor deposition (oCVD) conjugated polymers. For the first time, the oCVD growth kinetics for PEDOT is reported, which is governed by both T_{sub} and T_{oxi} during oCVD deposition. At a low T_{sub} of RT, the growth rate follows an Arrhenius relationship with an activation energy of approximately 1.9 eV at all T_{oxi} investigated; however, at higher T_{sub}, the growth rate becomes independent of T_{oxi}. Higher T_{sub} processing leads to enhanced crystalline structure in an edge-on packing orientation as well as longer conjugation length verified by FTIR evaluations and carrier mean free path analysis. Further, greater doping level in PEDOT also results from higher T_{sub}. The electrical properties of conductivity, carrier density and carrier mobility are significantly improved by the enhanced crystalline and chemical environmental structures in PEDOT grown at higher T_{sub} (still in the modest temperature regime ≤ 100 °C), which is highly favored in device applications as both flexible electrodes and other semiconductors (hole transporting layers in solar cells or active channel layers in field effect transistors). These findings of oCVD PEDOT growth kinetics and processing-structure-property relationship should contribute to the ongoing kinetic and carrier transport studies on PEDOT and other thiophene-based conjugated polymers, particularly processed using VPP and CVD techniques for various organic electrode and/or semiconductor applications.

Acknowledgements

References

[1] A.O. Patil, A.J. Heeger, F. Wudl, Optical-properties of conducting polymers, Chem. Rev. 88 (1) (1988) 183–200.

[2] A. Malinauskas, Chemical deposition of conducting polymers, Polymer 42 (9) (2001) 3957–3972.

[3] R.J. Kline, M.D. McGehee, Morphology and charge transport in conjugated polymer, Polym. Rev. 46 (1) (2006) 27–45.

[4] W.W. Li, A. Furlan, W.S.C. Roelofs, K.H. Hendriks, G.W.P. van Pruissen, M.M. Wienk, R.A.J. Janssen, Wide band gap diketopyrrolopyrrole-based conjugated polymers incorporating biphenyl units applied in polymer solar cells, Chem. Commun. 50 (6) (2014) 679–681.

[5] A.M. Coclite, R.M. Howden, D.C. Borrelli, C.D. Petruczok, R. Yang, J.L. Yaguee, A. Ugur, N. Chen, S. Lee, W.J. Jo, A. Liu, X. Wang, K.K. Gleason, 25th anniversary article: CVD polymers: A new paradigm for surface modification and device fabrication, Adv. Mater. 25 (38) (2013) 5392–5422.

[6] J.M. Xu, H.S.O. Chan, S.C. Ng, T.S. Chung, Polymers synthesized from (3-alkylthio) thiophenes by the FeCl3 oxidation method, Synth. Met. 132 (1) (2002) 63–69.

[7] M. Vosgueritchian, D.J. Lipomi, Z. Bao, Highly conductive and transparent PEDOT:PSS films with a fluorosurfactant for stretchable and flexible transparent electrodes, Adv. Funct. Mater. 22 (2) (2012) 421–428.

[8] J. Huang, P.F. Miller, J.C. de Mello, A.J. de Mello, D.D.C. Bradley, Influence of thermal treatment on the conductivity and morphology of PEDOT/PSS films, Synth. Met. 139 (3) (2003) 569–572.

[9] A.M. Nardes, M. Kemerink, R.A.J. Janssen, J.A.M. Bastiaansen, N.M.M. Kiggen, B.M.W. Langeveld, A. van Breemen, M.M. de Kok, Microscopic understanding of the anisotropic conductivity of PEDOT: PSS thin films, Adv. Mater. 19 (9) (2007) 1196-+.

[10] A.S. Alshammari, M. Shkunov, S.R.P. Silva, Correlation between wetting properties and electrical performance of solution processed PEDOT:PSS/CNT nano-composite thin films, Colloid Polym. Sci. 292 (3) (2014) 661–668.

[11] C. Duc, A. Vlandas, G.G. Malliaras, V. Senez, Wettability of PEDOT:PSS films, Soft Matter 12 (23) (2016) 5146–5153.

[12] K.K. Gleason, CVD Polymers: Fabrication of Organic Surfaces and Devices, Wiley, 2015.

[13] L.M.H. Groenewoud, G.H.M. Engbers, J.G.A. Terlingen, H. Wormeester, J. Feijen, Pulsed plasma polymerization of thiophene, Langmuir 16 (15) (2000) 6278–6286.

[14] N.V. Bhat, D.S. Wavhal, Preparation and characterization of plasma-polymerized thiophene films, J. Appl. Polym. Sci. 70 (1) (1998) 203–209.

[15] M.C. Barr, Polymers via chemical vapor deposition and their application to organic photovoltaics, Ph.D. Thesis, MIT, 2012.

[16] J. Kim, D. Sohn, Y. Sung, E.R. Kim, Fabrication and characterization of conductive polypyrrole thin film prepared by in situ vapor-phase polymerization, Synth. Met. 132 (3) (2003) 309–313.

[17] B. Winther-Jensen, K. West, Vapor-phase polymerization of 3,4-ethylenedioxythiophene: A route to highly conducting polymer surface layers, Macromolecules 37 (12) (2004) 4538–4543.

[18] S. Admassie, F.L. Zhang, A.G. Manoj, M. Svensson, M.R. Andersson, O. Inganas, A polymer photodiode using vapour-phase polymerized PEDOT as an anode, Sol. Energy Mater. Sol. Cells 90 (2) (2006) 133–141.

[19] R.M. Howden, E.D. McVay, K.K. Gleason, oCVD poly(3,4-ethylenedioxythiophene) conductivity and lifetime enhancement via acid rinse dopant exchange, J. Mater. Chem. A 1 (4) (2013) 1334–1340.

[20] M.C. Barr, J.A. Rowehl, R.R. Lunt, J. Xu, A. Wang, C.M. Boyce, S.G. Im, V. Bulovic, K.K. Gleason, Direct monolithic integration of organic photovoltaic circuits on unmodified paper, Adv. Mater. 23 (31) (2011) 3500-+.

[21] S. Lee, D.C. Paine, K.K. Gleason, Heavily doped poly(3,4-ethylenedioxythiophene) thin films with high carrier mobility deposited using oxidative CVD: conductivity stability and carrier transport, Adv. Funct. Mater. 24 (45) (2014) 7187–7196.

[22] R.M. Howden, E.J. Flores, V. Bulovic, K.K. Gleason, The application of oxidative chemical vapor deposited (oCVD) PEDOT to textured and non-planar photovoltaic device geometries for enhanced light trapping, Org. Electron. 14 (9) (2013) 2257–2268.

[23] M.C. Barr, R.M. Howden, R.R. Lunt, V. Bulovic, K.K. Gleason, Top-illuminated organic photovoltaics on a variety of opaque substrates with vapor-printed poly(3,4-ethylenedioxythiophene) top electrodes and MoO3 buffer layer, Adv. Energy Mater. 2 (11) (2012) 1404–1409.

[24] S.G. Im, D. Kusters, W. Choi, S.H. Baxamusa, M.C.M.v. de Sanden, K.K. Gleason, Conformal coverage of poly(3,4-ethylenedioxythiophene) films with tunable nanoporosity via oxidative chemical vapor deposition, ACS Nano 2 (9) (2008) 1959–1967.

[25] H. Chelawat, S. Vaddiraju, K. Gleason, Conformal, conducting poly(3,4-ethylenedioxythiophene) thin films deposited using bromine as the oxidant in a completely dry oxidative chemical vapor deposition process, Chem. Mat. 22 (9) (2010) 2864–2868.

[26] D.C. Borrelli, S. Lee, K.K. Gleason, Optoelectronic properties of polythiophene thin films and organic TFTs fabricated by oxidative chemical vapor deposition, J. Mater. Chem. C 2 (35) (2014) 7223–7231.

[27] S. Lee, D.C. Borrelli, K.K. Gleason, Air-stable polythiophene-based thin film transistors processed using oxidative chemical vapor deposition: Carrier transport and channel/metallization contact interface, Org. Electron. 33 (2016) 253–262.

[28] H. Park, R.M. Howden, M.C. Barr, V. Bulovic, K. Gleason, J. Kong, Organic solar cells with graphene electrodes and vapor printed poly(3,4-ethylenedioxythiophene) as the hole transporting layers, ACS Nano 6 (7) (2012) 6370–6377.

[29] W.J. Jo, J.T. Nelson, S. Chang, V. Bulović, S. Gradečak, M.S. Strano, K.K. Gleason, Oxidative chemical vapor deposition of neutral hole transporting polymer for enhanced solar cell efficiency and lifetime, Adv. Mater. 28 (30) (2016) 6399–6404.

[30] D. Bhattacharyya, K.K. Gleason, Single-step oxidative chemical vapor deposition of -COOH functional conducting copolymer and immobilization of biomolecule for sensor application, Chem. Mat. 23 (10) (2011) 2600–2605.

[31] D. Bhattacharyya, K. Senecal, P. Marek, A. Senecal, K.K. Gleason, High surface area flexible chemiresistive biosensor by oxidative chemical vapor deposition, Adv. Funct. Mater. 21 (22) (2011) 4328–4337.

[32] S. Vaddiraju, K.K. Gleason, Selective sensing of volatile organic compounds using novel conducting polymer-metal nanoparticle hybrids, Nanotechnology 21 (2010) 12.

[33] P. Kovacik, G.d. Hierro, W. Livernois, K.K. Gleason, Scale-up of oCVD: large-area conductive polymer thin films for next-generation electronics, Mater. Horiz. 2 (2) (2015) 221–227.

[34] J.P. Lock, S.G. Im, K.K. Gleason, Oxidative chemical vapor deposition of electrically conducting poly(3,4-ethylenedioxythiophene) films, Macromolecules 39 (16) (2006) 5326–5329.

[35] S.G. Im, K.K. Gleason, Systematic control of the electrical conductivity of poly(3,4-ethylenedioxythiophene) via oxidative chemical vapor deposition, Macromolecules 40 (18) (2007) 6552–6556.

[36] X.X. Wang, X. Zhang, L. Sun, D. Lee, S. Lee, M.H. Wang, J.J. Zhao, Y. Shao-Horn, M. Dinca, T. Palacios, K.K. Gleason, High electrical conductivity and carrier mobility in oCVD PEDOT thin films by engineered crystallization and acid treatment, Sci. Adv. 4 (2018) (9).

[37] F.C. Eversteyn, Chemical-reaction engineering in semiconductor industry, Philips

Research Reports 29 (1) (1974) 45–66.

[38] R.C. Jaeger, Introduction to Microelectronic Fabrication, Prentice Hall, 2002.

[39] T.A. Skotheim, J. Reynolds, Handbook of Conducting Polymers 2 Volume Set CRC Press, 2007.

[40] S. Rattan, P. Singhal, A.L. Verma, Synthesis of PEDOT:PSS (poly(3,4-ethylene-dioxythiophene))/poly(4-styrene sulfonate))/ ngps (nanographitic platelets) nanocomposites as chemiresistive sensors for detection of nitroaromatics, Polym. Eng. Sci. 53 (10) (2013) 2045–2052.

[41] S.V. Selvaganesh, J. Mathiyarasu, K.L.N. Phani, V. Yegnaraman, Chemical synthesis of PEDOT–Au nanocomposite, Nanoscale Res. Lett. 2 (11) (2007) 546–549.

[42] S.O. Kasap, Principles of Electronic Materials and Devices, McGraw-Hill, 2006.

[43] S. Lee, D.C. Paine, K.K. Gleason, Heavily doped poly(3,4-ethylenedioxythiophene) thin films with high carrier mobility deposited using oxidative CVD: Conductivity stability and carrier transport, Adv. Funct. Mater. (2014), https://doi.org/10.1002/adfm.201401282.

[44] S.H. Lee, K.K. Gleason, Enhanced optical property with tunable band gap of cross-linked PEDOT copolymers via oxidative chemical vapor deposition, Adv. Funct. Mater. 25 (1) (2015) 85–93.

[45] A. Ugur, F. Katmis, M. Li, L. Wu, Y. Zhu, K.K. Varanasi, K.K. Gleason, Low-dimensional conduction mechanisms in highly conductive and transparent conjugated polymers, Adv. Mater. 27 (31) (2015) 4604–4610.

[46] S. Lee, D.C. Borrelli, W.J. Jo, A.S. Reed, K.K. Gleason, Nanostructured unsubstituted polythiophene films deposited using oxidative chemical vapor deposition: hopping conduction and thermal stability, Adv. Mater. Interfaces 5 (2018) 9.

[47] Y.C. Cheng, R.J. Silbey, D.A. da Silva, J.P. Calbert, J. Cornil, J.L. Bredas, Three-dimensional band structure and bandlike mobility in oligoacene single crystals: A theoretical investigation, J. Chem. Phys. 118 (8) (2003) 3764–3774.

[48] S. Fratini, S. Ciuchi, Bandlike motion and mobility saturation in organic molecular semiconductors, Phys. Rev. Lett. 103 (2009) 26.

[49] V.J. Babu, S. Vempati, S. Ramakrishna, Conducting polyaniline-electrical charge transportation, No.01, Mater. Sci. Appl. vol. 04, (2013) 10.

[50] R.J. Kline, M.D. McGehee, Morphology and charge transport in conjugated polymers, J. Macromol. Sci., Part C 46 (1) (2006) 27–45.

[51] L. Zuppiroli, M.N. Bussac, S. Paschen, O. Chauvet, L. Forro, Hopping in disordered conducting polymers, Phys. Rev. B 50 (8) (1994) 5196–5203.

[52] S. Capaccioli, M. Lucchesi, P.A. Rolla, G. Ruggeri, Dielectric response analysis of a conducting polymer dominated by the hopping charge transport, J. Phys.: Condens. Matter 10 (25) (1998) 5595.

[53] G.C. Psarras, Hopping conductivity in polymer matrix–metal particles composites, Compos. A Appl. Sci. Manuf. 37 (10) (2006) 1545–1553.

[54] C. Hu, Modern Semiconductor Devices for Integrated Circuits, Prentice Hall, 2010.

[55] J. Hong, J. Paik, H. Hwang, S. Lee, A.J. deMello, K. No, The effect of growth temperature on physical properties of heavily doped ZnO: Al films, Phys. Status Solidi A-Appl. Mater. Sci. 206 (4) (2009) 697–703.

[56] E.T. Kang, K.G. Neoh, K.L. Tan, X-ray photoelectron spectroscopic studies of poly (2,2'-bithiophene) and its complexes, Phys. Rev. B 44 (19) (1991) 10461–10469.

[57] J. Lei, S. Rudenja, N. Magtoto, J.A. Kelber, Cu electrodeposition on Ru(0001): Perchlorate dissociation and its effects on Cu deposition, Thin Solid Films 497 (1–2) (2006) 121–129.

[58] C. Moustydesbuquoit, J. Riga, J.J. Verbist, Solid-state effects in the electronic-structure of ticl4 studied by XPS, J. Chem. Phys. 79 (1) (1983) 26–32.

[59] C. Moustydesbuquoit, J. Riga, J.J. Verbist, Electronic-structure of titanium(III) and titanium(IV) halides studied by solid-phase x-ray photoelectron-spectroscopy, Inorg. Chem. 26 (8) (1987) 1212–1217.

[60] H. Mori, K. Hasebe, N. Terano, Variation in oxidation state of titanium species on MgCl(2-)supported Ziegler catalyst and its correlation with kinetic behavior for propylene polymerization, Polymer 40 (6) (1999) 1389–1394.

[61] S.C. Ng, J.M. Xu, H.S.O. Chan, Synthesis and characterization of regioregular polymers containing substituted thienylene/bithienylene and phenylene repeating units, Macromolecules 33 (20) (2000) 7349–7358.

[62] A. Furlani, M.V. Russo, G. Polzonetti, K. Martin, H.H. Wang, J.R. Ferraro, Spectroscopic studies of fecl3-doped polymers of polyphenylacetylene, Appl. Spectrosc. 44 (2) (1990) 331–334.